BioSystems 97 (2009) 35–43

Contents lists available at ScienceDirect

BioSystems

journal homepage: www.elsevier.com/locate/biosystems

Neural model of frog ventilatory rhythmogenesis

Ginette Horcholle-Bossavit [a], Brigitte Quenet [b,*]

[a] UMR CNRS 7084, Laboratoire d'Electronique, ESPCI, 10 rue Vauquelin, 75005 Paris, France
[b] Equipe de Statistique Appliquée, ESPCI, 10 rue Vauquelin, 75005 Paris, France

ARTICLE INFO

Article history:
Received 24 September 2008
Received in revised form 9 April 2009
Accepted 9 April 2009

Keywords:
Frog ventilation
Neural population
Coupled oscillators
Rhythmogenesis
Pattern generator

ABSTRACT

In the adult frog respiratory system, periods of rhythmic movements of the buccal floor are interspersed by lung ventilation episodes. The ventilatory activity results from the interaction of two hypothesized oscillators in the brainstem. Here, we model these oscillators with two coupled neural networks, whose co-activation results in the emergence of new dynamics. One of the networks is built with "loop chains" of excitatory and inhibitory neurones producing periodic activities. We define two groups of excitatory neurones whose oscillatory antiphasic sums of activities represent output signals as possible motor commands towards antagonist buccal muscles. The other oscillator is a small network with a self-modulated excitatory input to an excitatory neurone whose episodic firings synchronise some neurones of the first network chains. When this oscillator is silent, the output signals exhibit only regular oscillations, and, when active, the synchronisation process reconfigures the output signals whose new features are representative of lung ventilation motor patterns. The biological interest of this formal model is illustrated by the persistence of the relevant dynamical features when perturbations are introduced in the model, i.e. dynamic noises and architecture modifications. The implementation of the networks with clock-driven continuous time neurones provides simulations with physiological time scales.

1. Introduction

Adult frogs exhibit prolonged periods of rhythmic ventilation of the buccal cavity, termed "buccal oscillations", interspersed by "breathing periods". Motor nerve patterns indicative of both buccal oscillations and lung ventilation persist in the frog *in vitro* brainstem preparation, showing that the capacity for their generation resides within the brainstem itself. Several sets of data support the hypothesis that breathing is driven by two anatomically distinct rhythm generators (Wilson et al., 2002, 2006). In addition recent studies suggest that circuits generating the respiratory rhythm in the mammalian brainstem may have evolved from vertebrate ancestors (Wilson et al., 2006). Studying the rhythm generating circuits of amphibians is likely to shed light on the fundamental properties of the mammalian respiratory circuit (Vasilakos et al., 2005). A model of rhythmogenesis in the frog ventilatory system (Bose et al., 2005) was based on two neurones of Morris–Lecar type, named "Buccal oscillator" (B) and "Lung oscillator" (L), respectively, driven together by seven equations. In the Bose model, each unit has its own oscillator properties. The coupling of these oscillatory units consists of an excitatory connection from L to B, and of an inhibitory connection from B to L, connection which is modulated by the potential of the buccal neurone. This modulated coupling produces a bi-stability between two oscillatory modes figuring buccal oscillations and lung episodes respectively. We propose a model which keeps two main features of the Bose model, i.e. (i) the excitatory–inhibitory interrelation between B and L oscillators, and (ii) the idea of a modulated input to L. Our model takes into account the experiments showing that after sectioning of the brainstem, L oscillator and B oscillator (Torgerson et al., 2001a) are separated in distinct segments, and the main features of their respective activities are maintained, i.e. regular oscillations for B and episodic activity for L. In the neurograms recorded from cranial nerves corresponding to the sectioned segments containing the B oscillator, the oscillation frequency is the same as in intact preparations (Wilson et al., 2002). The neurograms corresponding to L oscillator still exhibit episode occurrence, whose frequency is significantly lower than the frequency observed in the intact brainstem. These results strongly suggest that the occurrence of L episodes does not depend on B oscillator, as in the Bose model, but depends rather on L oscillator itself. It is the reason why, in our model, the modulation process driving the episodic activity of L depends on L activity. To give the model a higher physiological relevance, we considered each oscillator as a neural network. Modelling rhythm generators with neural populations offers the opportunity of defining sub-groups of neurones according to their activity phase relationships, thus configuring possible complex motor sequences. Our modelling approach also takes into account the conceptual distinction between the generation of rhythm and the generation

* Corresponding author. Tel.: +33 1 40 79 44 61.
E-mail address: brigitte.quenet@espci.fr (B. Quenet).

0303-2647/$ – see front matter © 2009 Elsevier Ireland Ltd. All rights reserved.
doi:10.1016/j.biosystems.2009.04.002

of output patterns, which seems meaningful from a physiological point of view (Rybak et al., 2006; Oku et al., 2008). In this paper, we develop a model of rhythm generation leading to output signals that can represent appropriate ventilatory motor commands. Such motor commands could be used for a recruitment process of specific motoneurone populations involved in oscillations of the buccal floor, and in the complex muscle sequence of a lung episode (Brett and Shelton, 1979; Sakakibara, 1984; Gdovin et al., 1998). In a first step, the model is implemented with discrete time McCulloch and Pitts neurones (MCP) (McCulloch and Pitts, 1943), because it is easier to analyse the relationship between the architecture and the dynamics in such networks (Horcholle-Bossavit et al., 2007). In a second step, the MCP are replaced by Izhikevich type neurones (Izhikevich, 2003) which give the model a biologically plausible time scale.

2. Methods

The model network is made of two coupled oscillators: the B oscillator, built on a structure based on loop chains, and the L oscillator made of a single loop. The reciprocal connections between L and B are such that L synchronises B neurones, and L is inhibited by B. This model network is implemented either with MCP neurones or Izhikevich type neurones.

2.1. MCP neurones

The MCP neurones are formal units with binary states: 0, equivalent to silence, or 1, equivalent to the emission of a spike when a neurone is firing. In the network, the state $S_i(k)$ of neurone i is updated at time step k, according to Eq. (1). This equation indicates that, at each time step k of a simulation the synaptic balance to neurone i is computed, and if it reaches the threshold θ,

$$\begin{aligned} &S_i(k) = 1, \quad \text{otherwise,} \quad S_i(k) = 0. \\ &S_i(k) = H\left(\sum_{j=1}^{N} w_{ij}\, S_j(k-\tau_{ij}) + E_i + \varepsilon r - \theta\right) \end{aligned} \tag{1}$$

where w_{ij} is the synaptic weight from neurone j to neurone i, τ_{ij} is the transmission delay from neurone j to neurone i: the running index j belongs to $[1, \ldots, N]$ with N the number of neurones in the network. E_i is an external input to neurone i. A stochastic factor is introduced at each time step as a standard normal random term r multiplied by a dynamical noise parameter ε, which is null in deterministic simulations H is the Heaviside function, whose value is zero if its argument is negative and 1 if its argument is positive or zero. In this model, all the synaptic delays are unit delays: $\tau_{ij} = 1$ and the synaptic weights w_{ij} are either zero or unitary: (+1) for excitatory connections or (−1) for inhibitory ones. The inputs E_i are either zero or excitatory (+1) and $\theta = 0.5$. The update rule is a synchronous rule, i.e. at each type step k, all the neurones ($i = 1, \ldots, N$) are updated according to Eq. (1).

2.2. Network of Izhikevich type neurones

The Izhikevich neurone captures many biological properties of realistic Hodgkin–Huxley type conductance-based models but with a greater simplicity in implementation (Izhikevich, 2004). In this model the potential of each neurone is given by a bi-dimensional system of Ordinary Differential Equations (ODE). Using a numerically stable 'leapfrog' integration method, the ODE equations for neurone i are defined in Eq. (2):

$$\begin{aligned} v_i(t) &= v_i(t-dt) + dt(0.04\, v_i(t-dt)^2 + 5\, v_i(t-dt) + 140 - u_i(t-dt) + I_i(t)) \\ u_i(t) &= u_i(t-dt) + dt(a(b\, v_i(t) - u_i(t-dt))) \end{aligned} \tag{2}$$

where the integration time step dt represents a biological time duration of 1 ms when it equals 1; $v_i(t)$ is the membrane potential in mV of neurone i and $u_i(t)$ is an auxiliary negative feedback variable at time t. Two parameters a and b define the neurone type, together with c and d, introduced for resetting $v_i(t)$ and $u_i(t)$, respectively when $v_i(t)$ is equal or higher than a reference value set at +30 mV. In this situation, the state of neuron i at time t is $S_i(t) = 1$, which represents its spike emission, and $S_i(t) = 0$ otherwise. The after-spike resetting is defined by the conditions in Eq. (3):

$$\begin{aligned} v_i &\leftarrow c \\ u_i &\leftarrow u_i + d \end{aligned} \tag{3}$$

With the following values for the parameters: $a = 0.02$, $b = 0.2$, $c = -65$, and $d = 8$, this model exhibits a tonic spiking behaviour in response to a steady input with a quasi-linear frequency–intensity relationship.

The Izhikevich network is build with the same architecture as in the MCP network, i.e. with same w_{ij}, τ_{ij}, and E_i, whatever i and j. Input and synaptic contributions to Izhikevich neurone i at time t are delivered through the variable $I_i(t)$ in Eq. (2). $I_i(t)$ is computed according to Eq. (4):

$$I_i(t) = I^{in} + I^{syn}(t) \tag{4}$$

The first term is a steady depolarizing current when $E_i > 0$:

$$I^{in} = I^{Dep} \tag{5}$$

where I^{Dep} is a value set in order to get a tonic spiking activity for neuron i, with an interspike time P. The value of P decreases when I^{Dep} increases.

The second term containing the synaptic contributions to neuron i is given in Eq. (6):

$$\begin{aligned} I^{syn}(t) = &\sum_{j=1}^{N} H(w_{ij})\, w_{ij}\, G^{ex}_{\max} S_j(t - \tau_{ij} Del^{ex}) + \sum_{k=1}^{N} H(-w_{ik}) w_{ik} G^{in}_{\max} S_k(t - \tau_{ik} Del^{in}) \\ &+ H(I^{syn}(t-dt)) I^{syn}(t-dt)(1-a^{ex}) + H(-I^{syn}(t-dt))\, I^{syn}(t-dt)(1-a^{in}) \end{aligned} \tag{6}$$

where $G^{ex}{}_{max}$ and $G^{in}{}_{max}$ are the respective maximal values of excitatory and inhibitory synaptic currents, whose temporal decay is an exponential time function with respective rates α^{ex} and α^{in}. Del^{ex} and Del^{in} are the respective transmission delays between a pre-synaptic spike ($S_j(t - \tau_{ij} Del^{ex}) = 1$ or $S_k(t - \tau_{ik} Del^{in}) = 1$) and the corresponding induced excitatory or inhibitory synaptic current in the post-synaptic neuron i.

The values of these six synaptic parameters are set in such a way that: (i) a neurone receiving an excitatory post-synaptic current at t_0: $G^{ex}{}_{max}\exp(-\alpha^{ex}(t-t_0))$ emits a spike at $t_0 + t_{ret}$, t_{ret} being the time of the spiking response to this excitation; (ii) a neurone receiving both an excitatory post-synaptic current at t_0: $G^{ex}{}_{max}\exp(-\alpha^{ex}(t-t_0))$ and an inhibitory post-synaptic current which is at t_0: $G^{in}{}_{max}\exp(-\alpha^{in}(t_0 - t_{in}))$, with $t_{in} < t_0$ the time of this incoming inhibitory current, remains silent; (iii) a neurone receiving both a depolarizing steady input current: I^{Dep} and an inhibitory post-synaptic current at t_0: $G^{in}{}_{max}\exp(-\alpha^{in}(t-t_0))$ is silent between t_0 and $t_0 + P$; (iv) an excitatory neuron emitting a spike induces a spike in a post-synaptic neuron at a time belonging to $[P - t_{ret}, P + t_{ret}]$.

When these conditions are satisfied, we get very similar activity maps in MCP and Izhikevich type neurones, with one time step in MCP network simulations corresponding to Pms and to P/dt integration time steps in Izhikevich network simulations.

2.3. B oscillator: a loop chain

In our model, the rhythmic activities corresponding to the B oscillator originate from a basic loop connecting three MCP neurones. This basic 3N loop is based on the connection 3×3 matrix W: [0 0 −1; 1 0 −1; 0 1 0]; all terms of the delay matrix T are equal to 1. When an excitatory unit input E_1 is applied to the first neurone of the chain, the 3N loop activity evolves towards a 5-time steps periodic attractor which is reached whatever the initial state. In order to build models with populations of oscillating neurones whose periodic activities are regularly phase lagged, the B network is organized as loop chains. Simulations showing neurone activities of MCP or Izhikevich networks were implemented in Matlab.

A chain of five 3N loops (Fig. 1Aa) leads to the activities shown in Fig. 1Ab. Each neurone, but the first one, is active during two successive time steps and silent during three successive time steps, with a phase lag of one time step between successive excitatory neurones in the chain. The first neurone which receives input $E_1 = 1$, is active during three successive time steps and silent during two successive time steps: this neurone is the "leader" (Wang and Slotine, 2006) of the chain. It drives the other neurones whose activities are distributed onto the five steps of the periodic dynamics: it results in a regular oscillation of the number of active excitatory neurones (Fig. 1Ac). When the same network is simulated with Izhikevich type neurones (Fig. 1B), the individual membrane potential $v_i(t)$ of neuron i exhibit action potentials and sub-threshold excitatory and inhibitory effects, according to the evolution of $I_i(t)$ (Fig. 1Ba, neuron 2: thick line for $v_2(t)$ and thin line for $I_2(t)$). The neurone firings, corresponding to the states $S_i(t) = 1$, exhibit the spatio-temporal patterns of $S_i(k) = 1$ in the MCP network, as shown in Fig. 1Ab and 1Bb. In the Izhikevich network, the output signal illustrated in Fig. 1Bc is computed by filtering the sum of the individual spikes (membrane potentials higher than −55 mV) of the excitatory neurones with a recursive filter based on a moving square window of width P/dt. This filter is applied in forward and backward directions, performing a zero-phase digital filtering (Gustafsson, 1996). As one time step in MCP network simulations corresponds to P/dt integration time steps in Izhikevich network simulations, with P about 100 ms and $dt = 0.125$ ms, the sequence illustrated in Fig. 1 corresponds to 40-time steps in the MCP network and to 32000 time steps in the Izhikevich network, i.e. 4 s. In these conditions, the frequency of the output signal, determined by P, is 2 Hz. This biologically plausible time scale is used for labelling the time axis in the MCP simulations.

2.4. L oscillator: a small modulated network

The part of the model corresponding to the L oscillator is based on two MCP neurones: an excitatory neurone l_1, and an inhibitory neurone l_2, connected by unitary connections. l_2 inhibits l_1 and itself (Fig. 2A inset). L exhibits a single

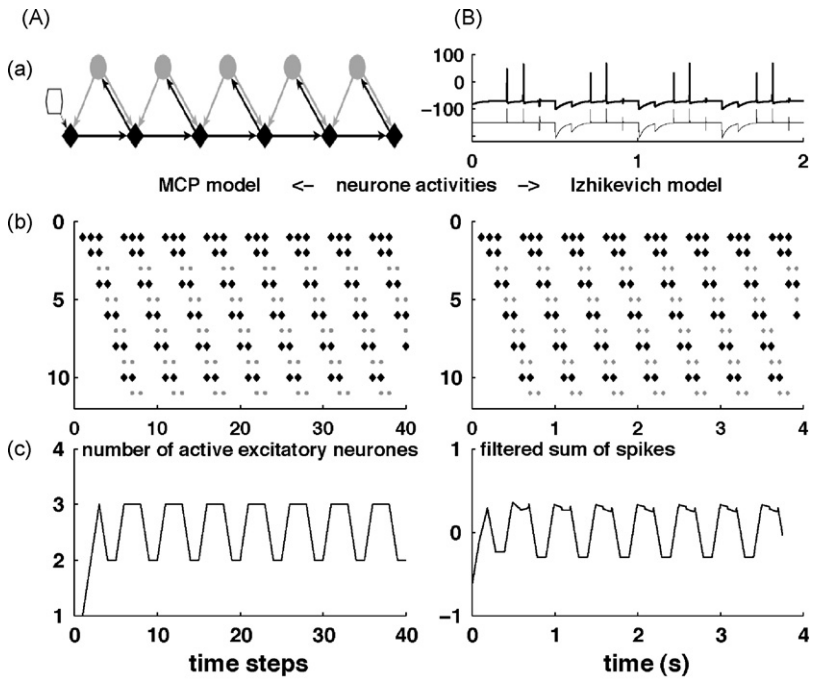

Fig. 1. 3N loop chain used in B oscillator. (Aa) Oriented graph of a chain of five 3N loops: neurones are either excitatory (black diamonds) or inhibitory (grey filled circle) with their respective excitatory (black arrows) and inhibitory (grey arrows) connections. The leader receives a unitary excitatory input E represented by a white hexagon. (Ab) Simulation showing the activities in the 3N loop chain with MCP neurones for 40-time steps: neural state 1 is indicated by black diamonds for excitatory neurones and grey dots for inhibitory ones. Vertical axis: neurone number. (Bb) Simulation showing the activities in the 3N loop chain with Izhikevich type neurones for 4 s: spikes are indicated by black diamonds for excitatory neurones and grey dots for inhibitory ones. Vertical axis: neurone number. (Ba) Evolution of neurone 2 membrane potential $v_2(t)$ (thick line) showing its spiking activity and its corresponding current $I_2(t)$ (thin line) for the two first seconds of the simulation. (Ac) Evolution of the "output signal" which is the number of active excitatory neurons in the MCP model. (Bc) Evolution of the "output signal" which is the filtered sum of the spikes (membrane potentials higher than −55 mV) of the Izhikevich excitatory neurones. Parameter values for Izhikevich model: $I^{Dep} = 4.8$; $G^{ex}{}_{max} = 50$; $G^{in}{}_{max} = 30$; $\alpha^{ex} = 1\ ms^{-1}$; $\alpha^{in} = 0.026\ ms^{-1}$; $Del^{ex} = 96.7$ ms; $Del^{in} = 95.1$ ms; $dt = 0.125$ ms.

attractor with a period equals to 2, when both I_1 and I_2 receive a unitary external excitatory input. When I_2 receives an external input $E_2 = 1$ and I_1 receives a modulated excitation, other attractors may appear depending on the synaptic balance on I_1.

In order to modulate I_1 activity, we define a modulated excitatory input received by I_1, $Em_{I1}(t)$, which depends on I_1 activity. An example of temporal evolution of $Em_{I1}(t)$ is illustrated in Fig. 2. Active periods of I_1 are characterized at each time step of the simulation by a variable $Ac(t)$ which represents the counter of I_1 "spikes" number, i.e. $S_{I1} = 1$, whose maximal value is fixed at $MaxAc$. $Ac(t)$ is updated according to Eq. (7), where H is the Heaviside function.

$$Ac(t) = [1 - H(Ac(t-1) - MaxAc)](S_{I1}(t-1) + Ac(t-1)) \tag{7}$$

The counter Ac is active with the first occurrence of $S_{I1} = 1$ and is reset to 0 when $MaxAc$ is reached by Ac. At time t, $Em_{I1}(t) > 0$ is the sum of three terms: (i) the excitation increase ($\beta Em_{I1}(t-1)$) when I_1 is silent, with the kinetic parameter $\beta > 1$, (ii) a reset value $Em_0 > 0$ when Ac reaches the predefined constant $MaxAc$, (iii) a modulation noise parameter γ, multiplying x, a uniform random real variable between (−0.5) and (0.5). $Em_{I1}(t)$ is updated according to Eq. (8):

$$\begin{aligned} Em_{I1}(t) = {} & [1 - H(Ac(t-1) - MaxAc)]\,(\beta Em_{I1}(t-1)) \\ & + [H(Ac(t-1) - MaxAc)]\,Em_0 + \gamma\, x \end{aligned} \tag{8}$$

The excitatory input $Em_{I1}(t)$ increases until $Ac(t-1)$ equals $MaxAc$, when the reset occurs (Fig. 2A). The minimal positive value for $Em_{I1}(t)$ is set at $Em_0 = 0.1$ in all simulations. A "lung episode", related to I_1 activity, begins when Ac equals 1 and ends when Ac equals $MaxAc \geq 1$. The value of $MaxAc$ can be modified after each Ac reset by an additional stochastic term, which is a uniform random real variable between (−0.5) and (0.5) multiplied by the duration noise parameter δ. The simulation shown in Fig. 2 illustrates two examples of I_1 episodes, with dynamical noise only ($\varepsilon = 0.06$, $\gamma = 0$, $\delta = 0$).

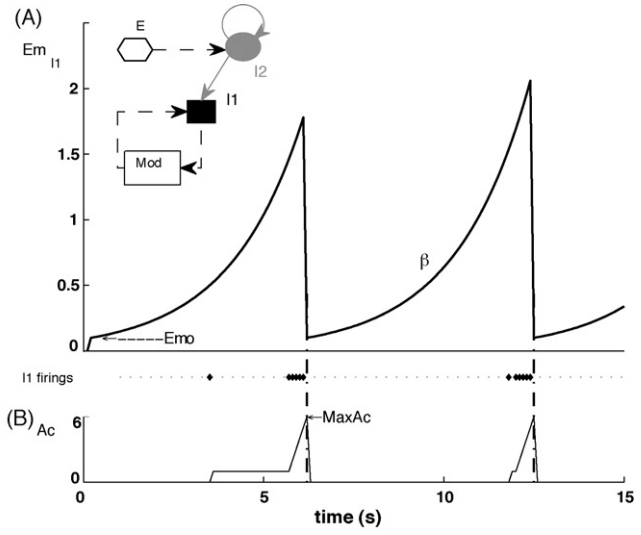

Fig. 2. Modulated L oscillator. (A) Temporal evolution of the modulated excitation Em_{I1}. Inset: oriented graph of L network, where "Mod" represents the auto-modulation function. (B) Temporal evolution of Ac, measuring the activity of I_1, reset when Ac reaches $MaxAc$. Black diamonds indicate state 1 for I_1 (I_1 firings). Parameter values: $\beta = 1.05$, $MaxAc = 6$, $\gamma = 0$, $\varepsilon = 0.06$, $\delta = 0$, $Em_0 = 0.1$.

2.5. Ventilatory model LB: connecting L and B networks

The model LB comprises the L network and the B network built as one chain of five loops. In the model, all synaptic weights (connection matrix and inputs) are unitary when non-zero, except the modulated excitatory input Em_{I1} to I_1. Neurone labelled I_3, neither active nor connected to the network is introduced for graphical clarity in the raster plots. Fig. 3Ac shows the graph of the model with the corresponding connectivity matrix W_{LB1} (Fig. 3Aa) and input vector E_{LB1} (Fig. 3Ab). Neurone I_1 receives connections from all the inhibitory neurones of B and sends excitatory connections to each neurone of B (Fig. 3Ac).

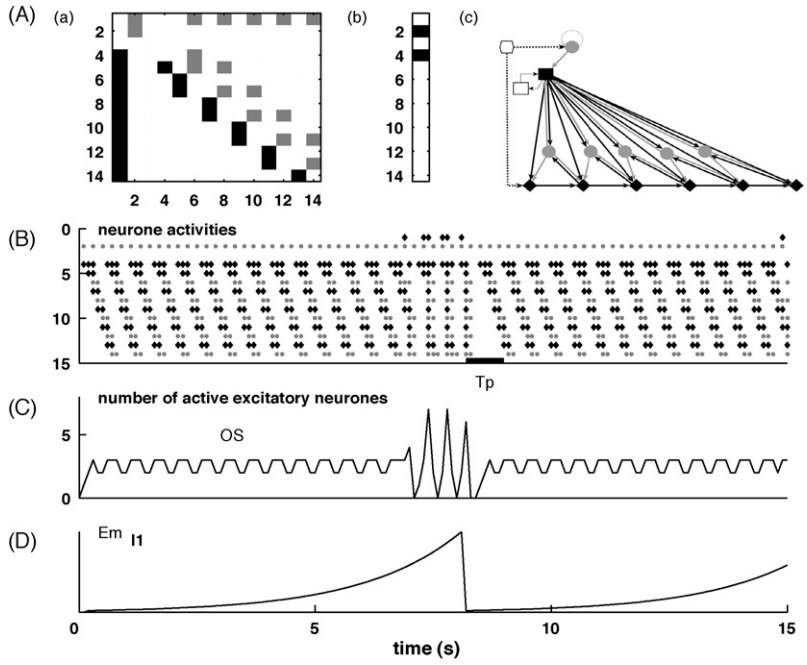

Fig. 3. LB network model: connecting L and B. (Aa) Connectivity matrix of the LB model connecting the oscillators L and B with excitatory (black squares), inhibitory (grey squares) and null connections (white). B excitatory neurones are numbered: 4 (leader), 5, 7, 9, 11, 13. B inhibitory neurones are numbered: 6, 8, 10, 12, 14. (Ab) Input vector with two excitatory inputs from *E*: to l_2 and to b_4 (4th neurone of LB network). (Ac) Corresponding oriented graph. Excitatory (black diamonds) or inhibitory (grey filled circles) neurones with their excitatory (black arrows) and inhibitory (grey arrows) connections. (B) Simulations of network activity: neural state 1 (firings) indicated by black diamonds for excitatory neurones and grey dots for inhibitory ones. Note that when l_1 is active the B neurones are synchronised. (C) Output signal *OS* of the network showing "buccal oscillation" and a "lung episode". (D) Temporal evolution of the modulated excitation Em_{l1}. Parameter values: $\beta = 1.05$, $MaxAc = 6$, $\gamma = 0$, $\varepsilon = 0$, $\delta = 6$, $Em_0 = 0.1$.

3. Results

3.1. Dynamics of model LB: buccal oscillation and episodic lung synchronisation

Two main features of the network dynamics are illustrated in Fig. 3B and C. When l_1 is silent, the dynamics exhibit phase lagged activities of the B neurones (Fig. 3B) corresponding to small regular oscillations of the output signal *OS*, the number of active excitatory neurones (Fig. 3C), i.e. B excitatory neurones and l_1. When l_1 is active, the neurones are synchronised and *OS* exhibits large amplitude oscillations. A transition period (*Tp*) appears after the synchronisation process due to l_1 activity, then the periodic dynamics resume (Fig. 3B). This transition period corresponds to the time necessary for the excitation to propagate along the chain. Fig. 3D shows the temporal evolution of Em_{l1}. The initiation of a lung episode needs a value of Em_{l1} which compensates the inhibition l_1 receives from l_2 and from the B inhibitory neurones. Longer simulations without any noise show a regular occurrence of lung episodes, whose frequency of occurrence and duration depend on the parameters β and *MaxAc* of the modulated excitation (Fig. 4A). When the value of β parameter is reduced, the time interval between two lung episodes is lengthened (Fig. 4Ab). When the value of *MaxAc* parameter is reduced, the lung episode duration is reduced (Fig. 4Ac). Since the biological neural dynamics are non-deterministic, stochastic behaviour is introduced in the model through three noise factors: the dynamical noise ε, the modulation noise γ and the duration noise δ. Simulations with the same sets of parameters but additional noises ($\varepsilon = 0.15$, $\gamma = 0.15$, $\delta = 6$) exhibit lung episodes with variable duration and occurrence frequency (Fig. 4B), like in physiological recordings (McLean et al., 1995; Torgerson et al., 2001a; Broch et al., 2002). These lung episodes may contain several synchronizing events, which appear as successive peaks in *OS*, and in some instances (Fig. 4Ba and Bc) lung activity appears as a single peak (Reid and Milsom, 1998). Noise affects the network dynamics and some disturbances appear in both buccal oscillations and lung episodes. Importantly, the introduction of noise allows the model to retain its two main properties: buccal rhythm and the occurrence of lung bursts. A quantitative analysis of the relationships between the duration of the lung episodes and *MaxAc* on one hand, and their occurrence frequency and β on the other hand, are illustrated in Fig. 5A and 5B, respectively. With the time scale defined in Section 2 (Fig. 1), when *MaxAc* varies from 2 to 10, the duration increases linearly from 0.9 s to 2.35 s; when β varies from 1.01 to 1.1, the frequency increases linearly from 1.6 to 19 min^{-1}. These values compare with the experimental values (McLean et al., 1995; Torgerson et al., 2001a; Broch et al., 2002; Oku et al., 2008).

3.2. Two antiphasic sub-populations

In our model based on populations of neurones, it is possible to increase the population size either by increasing the number of loops in a chain or by increasing the number of chains. When adding loops in the chains, there is an increase in the transition period *Tp*; by contrast, when the number of chains is increased, without adding any new loop to the chains, *Tp* is constant. Here, the B neural population is increased by adding one loop in the chain and adding a second 6-loop chain, in order to define two subgroups of excitatory neurones of same size. The connection matrix and input vector of the corresponding LB model are shown in Fig. 6Aa and Ab. This matrix duplicates the connection matrix of Fig. 3Aa with an additional loop for the B population, and is complemented with appropriate inhibitory reciprocal connections between the two chains, in such a way that their activities are phase-locked. In the population of B neurones, two subgroups, *Bc* and *Bd*, in reference to "buccal constriction" and "buccal dilation" which involve antiphasic muscle activities (Kogo et al., 1994; Vasilakos et al., 2005)

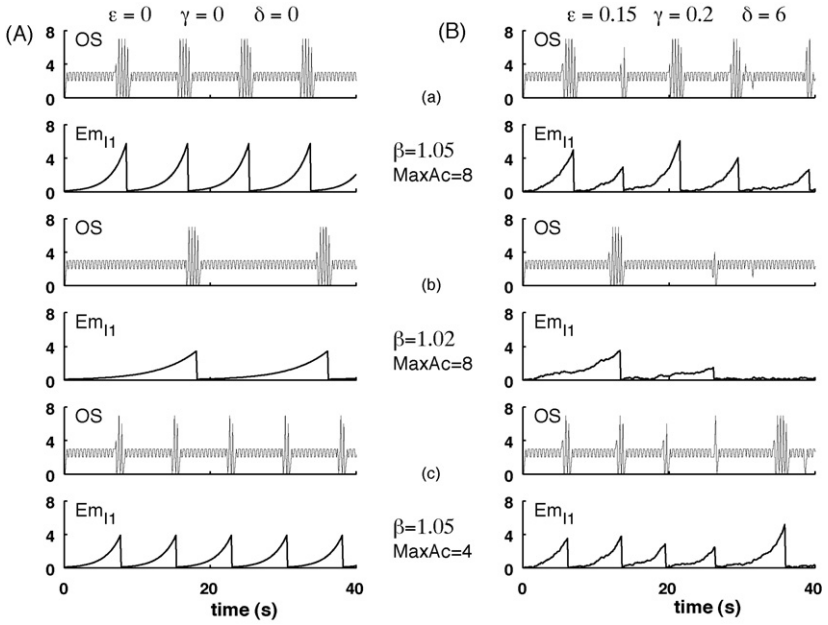

Fig. 4. Parameters determining duration and frequency of "lung episodes". (Aa–c and Ba–c) Upper graph: temporal evolution of *OS* showing lung episodes; lower graph: temporal evolution of Em_{l1} With the respective parameter values: A: without noise $\gamma = 0$, $\varepsilon = 0$, $\delta = 0$ and B: with noise $\gamma = 0.2$, $\varepsilon = 0.15$, $\delta = 6$. a: $\beta = 1.05$, $MaxAc = 8$, b: $\beta = 1.02$, $MaxAc = 8$, c: $\beta = 1.05$, $MaxAc = 4$.

are selected, as shown in Fig. 6Ac. Taking into account the conceptual distinction between the rhythm generator (RG) and the pattern generator (PG), we define the RG as the network made by L and two leaders of the chains (Fig. 6Ac). The pattern generator PG contains all the other neurones. The excitatory neurones defining the two groups *Bc* and *Bd* are selected in order to get two out-of-phase, almost antiphasic, output signals OS_{Bc} and OS_{Bd} (Fig. 6B and C) when l_1 is silent. All the B excitatory neurones receive an excitation from l_1 and are synchronised by this neurone during a lung episode, while in the inhibitory population of B, only inhibitory *Bc* neurones receive a connection from l_1 this produces small phase lags between OS_{Bc} and OS_{Bd} during lung episodes (Fig. 6B and C), l_1 activity being included in the OS_{Bc}. The phase relationships between

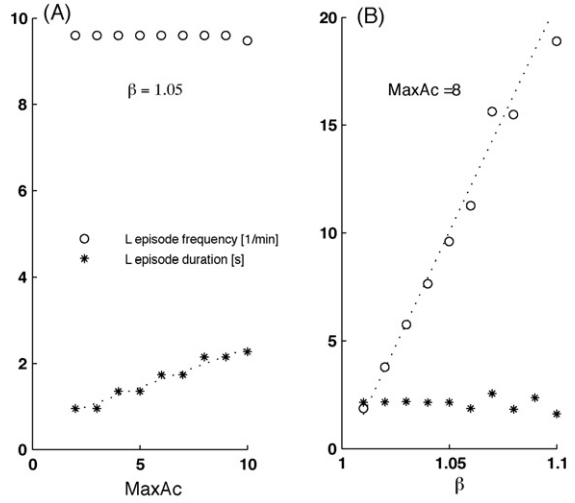

Fig. 5. L episode frequency and duration depend linearly on β and *MaxAc*. (A) With a fixed value of $\beta = 1.05$ and *MaxAc* varying from 2 to 10, the L episode frequency is stable around 9.6 min^{-1} and the duration increases linearly from 0.9 s to 2.35 s. (B) With a fixed value of $MaxAc = 8$ and β varying from 1.01 to 1.1, the L episode duration is stable around 2.15 s and the frequency increases linearly from 1.6 to 19 min^{-1}. Parameter values: $\gamma = 0$, $\varepsilon = 0$, $\delta = 0$, $Em_0 = 0.1$.

OS_{Bc} and OS_{Bd} are maintained when the three types of noise are present.

3.3. Architecture modifications

In the LB model, the temporal evolution of OS_{Bc} and OS_{Bd} results from the strictly organized network architecture based on loop chains. Does this architecture tolerate some flexibility while keeping the two crucial features: buccal regular antiphasic oscillations and episodic lung firings? In order to test the effects of some flexibility, we introduce perturbations in the network and evaluate their impact on the network dynamics and the output signals. The modifications are introduced by random suppression of some existing connections and random addition of new excitatory or inhibitory connections, whose weight w is fixed with this condition: $0 < |w| < 1$. The connection matrix shown in Fig. 7Ab illustrates an example of such modifications affecting the basic connection matrix shown in Fig. 7Aa (same matrix as in Fig. 6Aa and Ab): from the 76 original connections, 9 are suppressed and 41 new connections with $|w| = 0.15$ are added, thus, the matrix is affected by 50 modifications. Fig. 7B and C illustrate the effects of these architectural modifications: both regular buccal oscillatory behaviour with antiphasic Bc and Bd activities and the occurrence of lung episodes are retained. The critical point for the presence of these features is the continuity of excitation linking the loops in at least one of the chains.

3.4. Separation of L and B in model LB

Simulations of L and B dynamics have been performed after suppression of the connections between L and B (Fig. 8A), mimicking the experimental separation of L and B oscillators in the frog brainstem (Torgerson et al., 2001a; Wilson et al., 2002). Since in our model the modulation of the l_1 excitation depends on l_1 activity only, lung episodes do occur at the level of the isolated L (Fig. 8B and OS_{l1} in C), with a frequency and duration that mainly depend on new values of β and *MaxAc* parameters. In this situation, where l_1 activity is excluded from OS_{Bc}, the frequency of the antiphasic buccal oscillations of OS_{Bc}, and OS_{Bd} does not change (Fig. 8C).

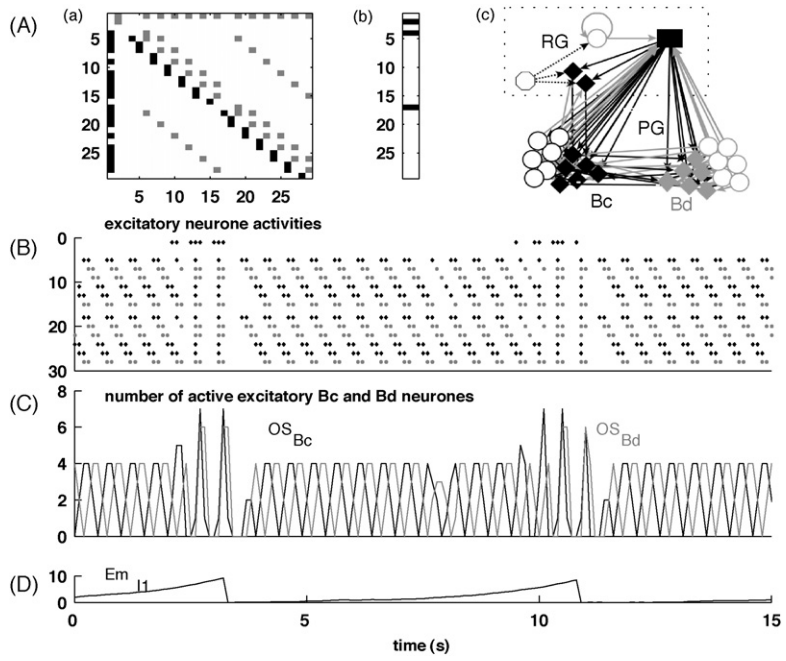

Fig. 6. Antiphasic OS_{Bc} and OS_{Bd} in LB model. (Aa) Connectivity matrix of LB model build with two chains of 6 loops linked by reciprocal inhibitory connections: excitatory (black squares), inhibitory (grey squares) and null connections (white). Bc excitatory neurones are numbered: 5, 11, 13, 18, 24, and 26. Bc inhibitory neurones are numbered: 6, 12, 14, 19, 25, and 27. Bd excitatory neurones are numbered: 7, 9, 15, 20, 22, and 28. Bd inhibitory neurones are numbered: 8, 10, 16, 21, 23, and 29. (Ab) Input vector with three excitatory inputs: to l_2 and to the two leaders b_4 (4th neurone of LB network) and b_{17} (17th neurone of LB network). (Ac) Oriented graph of LB model: RG: rhythm generator, containing l_2, the leaders b_4 and b_{17}, receiving a constant external input and l_1, with its modulated excitation (not shown). PG: pattern generator, containing two sub-groups of neurones identified as *Bc* and *Bd*. *Bc* group: excitatory neurones (black diamonds) and inhibitory neurones (black empty circles) *Bd* group: excitatory neurones (grey diamonds) and inhibitory neurones (grey empty circles). l_1 excitatory connections project to *Bc* and *Bd* neurones but the *Bd* inhibitory neurones. (B) LB excitatory neurone activities: black diamonds for excitatory neurones *Bc* and l_1, and grey diamonds for excitatory neurones *Bd*. (C) Corresponding OS_{Bc} (black line), the number of active excitatory *Bc* neurones ($+l_1$) and OS_{Bd} (grey line), the number of active excitatory *Bd* neurones. (D) Temporal evolution of the modulated excitation Em_{l1}. Parameter values: $\beta = 1.05$, $MaxAc = 8$, $\gamma = 0.2$, $\varepsilon = 0.15$, $\delta = 6$, $Em_0 = 0.1$.

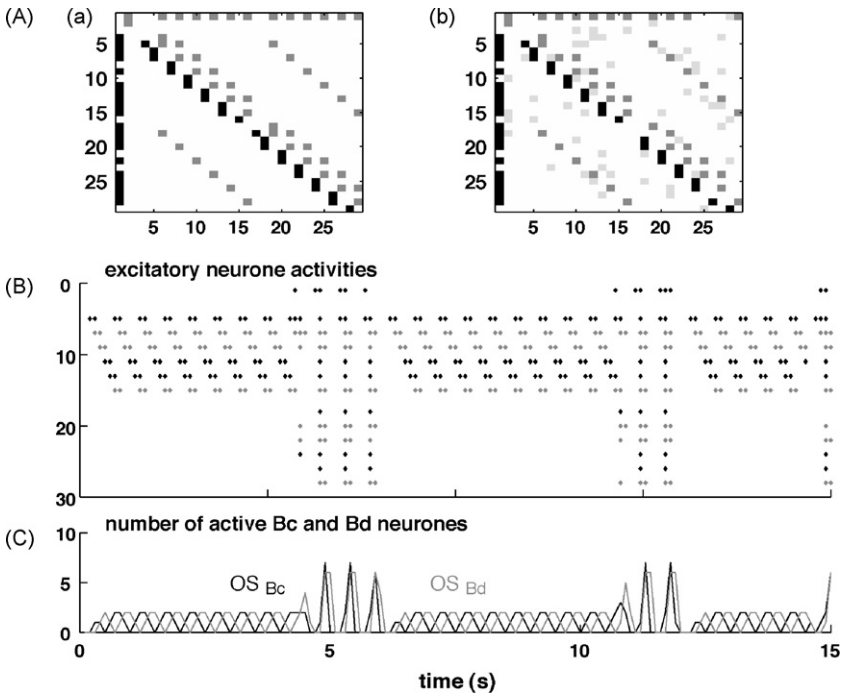

Fig. 7. Effects of modifications of the network architecture. (Aa) Connectivity matrix of LB model build with two chains of 6 loops linked by reciprocal inhibitory connections: excitatory (black squares), inhibitory (grey squares) and null connections (white). (Ab) Same basic matrix with 50 modified connections: random suppression of some existing connections and random addition of new excitatory or inhibitory connections whose weight is set at a value of 0.15. (B) Excitatory neurone activities of the LB model: black diamonds for neurones *Bc* and l_1, and grey diamonds for neurones *Bd*. (C) Number of active excitatory neurones *Bc* ($+l_1$) and *Bd*, i.e. OS_{Bc} (black line) and OS_{Bd} (grey line), respectively. Parameter values: $\beta = 1.05$, $MaxAc = 8$, $\gamma = 0.2$, $\varepsilon = 0.15$, $\delta = 6$, $Em_0 = 0.1$.

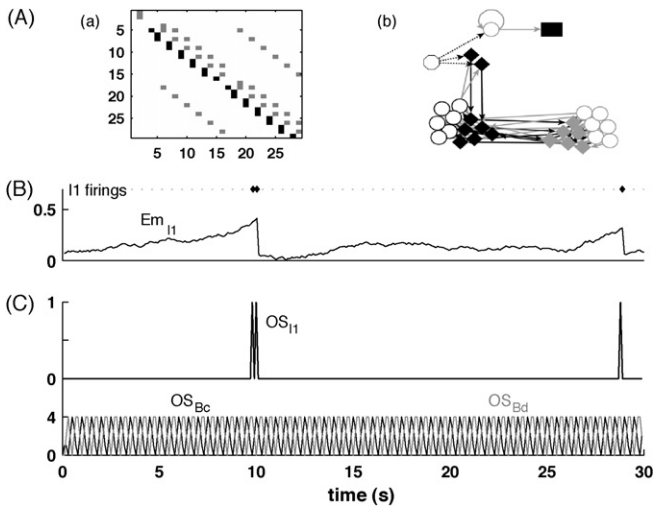

Fig. 8. L and B separation. (Aa) Connectivity matrix of the network when L and B oscillators are disconnected: excitatory connections (black squares) and inhibitory connections (grey squares), null connections (white). (Ab) Graph of the disconnected oscillators: B network with groups of *Bc* and *Bd* neurones shown as connected nuclei (black diamonds for *Bc* excitatory neurones, grey diamonds for *Bd* excitatory neurones, and empty circles for inhibitory neurones), without any connection with L oscillator (l_1: black rectangle and l_2: empty circle with auto-connection; modulation not shown). (B) l_1 firings (black diamonds) resulting from the auto-modulated excitation Em_{l1} (black line). "lung episodes" occurs corresponding to l_1 episodic firings. (C) B regular oscillations with antiphasic OS_{Bc} (black line) and OS_{Bd} (grey line). Parameter values: $\beta = 1.018$, $MaxAc = 2$, $\gamma = 0.05$, $\varepsilon = 0.05$, $\delta = 2$, $Em_0 = 0.1$.

3.5. Dynamics of LB with Izhikevich neurones

The model LB is implemented with Izhikevich neurones using the architecture defined by the matrix of Fig. 7Ab. Fig. 9 illustrates the dynamics of this model. The activity of excitatory neurones is shown as raster plots of their action potentials in Fig. 9A. An action potential corresponding to state 1 for MCP neurones, the raster plot of Izhikevich neurones exhibits a spatio-temporal activity map very similar to the MCP neurones map (compare with Fig. 7B). Fig. 9B illustrates, for l_1 and two excitatory B neurones, the time evolution of their membrane potentials $v_i(t)$ (thick line), showing their spikes, and the corresponding current $I_i(t)$) (thin line). The sums of the individual spikes (membrane potentials higher than −55 mV) of the *Bc* and *Bd* excitatory neurones, *Sum Bc* (including l_1) and *Sum Bd*, show the phase lagged dynamics of the two groups (Fig. 9C). In order to compute output signals similar to the signals OS_{Bc} and OS_{Bd} of Fig. 7C, these sums are filtered as in Fig. 1Bc. This processing provides the two respective output signals FS_{Bc} and FS_{Bd}, which are comparable to OS_{Bc} and OS_{Bd}, with both antiphasic buccal oscillations and lung episodes, with an adapted value of β in order to take into account the number of integration time steps.

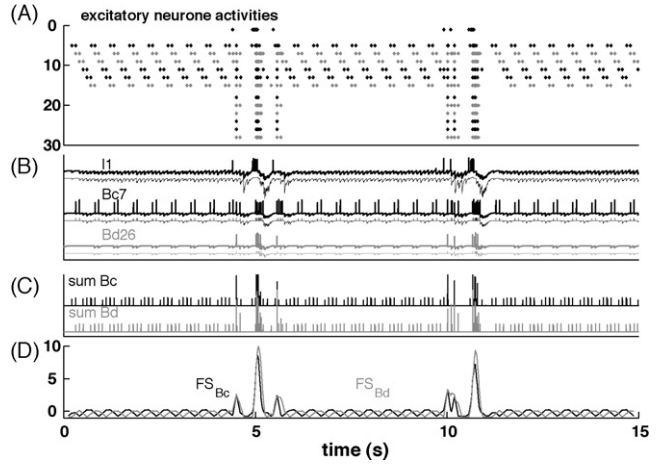

Fig. 9. LB model implemented with Izhikevich neurones. (A) Excitatory neurone activities of the LB model (same architecture as in (*Ab*)): spikes are indicated by black diamonds for excitatory neurones from the *Bc* group and l_1, and grey diamonds for excitatory neurones from the *Bd* group (compare with (B)). (B) Neurone l_1 and two other neurones, one in *Bc* group (*Bc7*) and one in *Bd* group (*Bd26*): evolution of membrane potential $v_i(t)$ (thick line) showing their spiking activity and their respective current $I_i(t)$ (thin line). (C) Sums of the spikes (membrane potentials higher than −55 mV) of the excitatory neurones: *sum Bc* (black line) and *sum Bd* (grey line) for neurones *Bc* (+l_1) and neurones *Bd*, respectively. (D) FS_{Bc} (black line) and FS_{Bd} (grey line) are the filtered sums of spikes; compare with OS_{Bc} and OS_{Bd} in (C). Parameter values: $\beta = 1.00013$, $MaxAc = 8$, $\gamma = 0.002$, $\varepsilon = 0$, $\delta = 0$, $Em_0 = 0.1$. Other parameters: same as in Fig. 1.

4. Discussion

4.1. Advantages of neural populations for modelling pattern generation

Our network model implemented either with MCP or Izhikevich neurones is built-in order to account for the basic physiological behaviours observed in the frog ventilatory system: (i) a neural oscillation at the origin of the rhythmic buccal floor movements with antiphasic activities of motoneurones projecting to antagonist muscles; (ii) some episodic neural activities which produce lung inflation or deflation (Vitalis and Shelton, 1990) through stronger buccal muscle contractions with narial and glottis contributions. To our knowledge, there are nor available data about the synaptic organisation of the frog respiratory network, neither precise information about the intrinsic properties of its pre-motor neurones: therefore, we have chosen to build the simplest network able to achieve both functions owing to the following features: a loop chain architecture responsible for buccal rhythmic distributed activities and a modulated excitation which episodically recruits lung excitatory neurone and synchronises B neurones. With the model neural population, it is possible to define a rhythm generator and a pattern generator, this matches the two conceptually levels considered in the frog brainstem (Rybak et al., 2006; Oku et al., 2008): in our model, the B neurones which contribute to the output signals belong to the pattern generator. The output signals of the models are defined as the number of selected active excitatory neurones in order to get the appropriate patterns for functional motor sequences: two sub-populations can be defined in B network, in such a way that their respective numbers of active neurones produce two almost antiphasic output signals. There are other advantages of dealing with neural units when building ventilation models. It is possible: (i) to consider a variety of network architectures, for instance, here B is made of one or two chains with various numbers of loops, (ii) to insert modifications in the strict regularity of the initial network topologies, which introduce biological likelihood. In the B neural population, excitatory neurones that are chained propagate an "oscillating wave" resulting in global regular rhythmic activity. Interestingly, a biological counterpart of such a network topology is suggested by a recent study of mice brainstem slices containing functional respiratory networks (Hartelt et al., 2008). Through optical recordings, mapping the neurones and their connections was used to generate wiring diagrams of the network, which is organized as chains of small clusters of a few neurones. In the MCP network the noise factor ε introduces fluctuations in the synaptic balance figuring communication defects between the neurones. In the Izhikevich network, a built-in property of the model introduces fluctuations in the membrane potentials and results in jitter affecting the spike timing.

4.2. Advantages of the modulated excitation on l_1

The deterministic modulated excitation Em_{l1} produces regular occurrence of lung episodes. It is possible to set the parameters and *MaxAc* in order to fully control occurrence frequency and pattern representing "breathing periods". A variety of possible patterns, including monophasic, biphasic or polyphasic peaks, can be obtained according to selected sets of β and *MaxAc*. Stochastic factors γ and δ introduces variability in the modulated excitation on l_1 and, therefore, in occurrence frequency and patterns of lung episodes. The effects of these factors on the modulated excitation indicate that a precise temporal evolution of Em_{l1} is not critical for the bi-stability of the network dynamics. As the modulated excitation is built independently from B activity, when L is separated from B, we get intermittent breathing episodes corresponding to l_1 activity.

4.3. Comparison with biological breathing patterns

The output signal patterns produced by the model are reminiscent of the various patterns observed in neurograms from *in vitro* preparations (Kogo et al., 1994; Reid and Milsom, 1998). In addition, the fact that such neurograms exhibit activity patterns which match the motor sequences observed in intact preparations (Vasilakos et al., 2005, 2006) suggests that the main driving input for the ventilatory system is provided by central chemoreceptors whose activity depends on normocapnia or hypercapnia (Torgerson et al., 2001b; Taylor et al., 2003). Our modulation rule could correspond to recruitment and de-recruitment processes of excitatory central chemoreceptors. Increasing β could correspond to a faster recruitment of such chemoreceptors, for instance with hypercapnia. Blocking the effects of such an excitatory recruitment would result in the suppression of lung burst activity (Chen and Hedrick, 2008). When brainstem segments containing L and B networks, respectively, are anatomically separated, L burst occurrence frequency is significantly lower than the frequency observed in the intact brainstem: our model may account for this observation provided a smaller value of β, corresponding to a smaller chemoreceptor population contained in the isolated L segment. The noise factor γ could represent fluctuations in the population of active central chemoreceptors. The noise factor δ could correspond to modifications of l_1 intrinsic properties by a neuromodulator (see Chen and Hedrick, 2008 for substance P effects) able to lengthen l_1 bursts.

The output signals OS_{Bc} and OS_{Bd} are antiphasic during buccal oscillations and slightly phased lagged during lung episodes. Higher amplitudes of OS_{Bc} and OS_{Bd} during lung episodes may account for both stronger buccal muscle contraction and recruitment of muscles responsible for glottis and narial movements (Kogo et al., 1994; Sakakibara, 1984).

4.4. Biological time scale

In order to compare the frequency and duration of buccal and breathing periods in the output signals with the corresponding physiological recordings, we calibrate the simulation time in terms of biological time. The Izhikevich neurone introduces a biologically plausible time scale in simulations, since the parameters in the difference equations (Eq. (2)) are calibrated for a time step *dt* in ms. The period of the B oscillation lasts for five update time steps in an MCP network which corresponds to 5*P*, i.e. to 500 ms, in the Izhikevich model. With this time scale, *B* frequency is 2 Hz. This frequency is of the order of magnitude of the frequency observed in recordings from adult frogs (see Table 1 in Vitalis and Shelton, 1990, and Fig. 5A in Vasilakos et al., 2005). Moreover, since in our model the buccal frequency is based on *P*, which depends on I^{Dep} value and on the intrinsic properties of the Izhikevich neurone, the minimal value for this frequency is about 1 Hz for the selected neuron (*a*, *b*, *c* and *d* given in methods). This Izhikevich model is a simple regular spiking neurone, but another model could be implemented in order to adapt the network dynamics to precise physiological data. The modulation parameter β and the reset parameter *MaxAc* can be adjusted at values which produce occurrence and duration of breathing periods corresponding to various physiological situations, stage and species (see Fig. 5). In simulations with Izhikevich neurones, there is an access to the temporal evolution of membrane potentials, revealing spikes and synaptic currents of each neurone that are comparable to physiological recordings. A recent study (Oku et al., 2008) shows that some respiratory neurones extracellularly recorded in the frog respiratory centres fire during both buccal and lung activities, while other ones fire only during lung episodes, these observations are similar to the simulated activities of Bc_7 or Bd_{26} and l_1 shown in Fig. 9. An additional advantage of dealing with Izhikevich neurones is the possible choice of their intrinsic properties. For instance, a bursting type neurone implemented in the model rather than the tonic spiking presented here could improve the robustness of the rhythm generation as suggested in a recent study (Purvis et al., 2007). The next step of this theoretical approach of the respiratory rhythm generation consists of using the *Bc* and *Bd* output signals produced by the present network as inputs to another network built with various threshold Izhikevich 'motoneurones' activated through a recruitment process, in order to model the motor patterns. The validation of a specific model, with appropriate parameters, will rely upon quantitative comparison between simulated motor signals and physiological neurograms in a particular biological preparation.

Acknowledgements

We are grateful to Dr. Christian Straus whose experimental works and questions are at the basis of the present theoretical work. His critical reading of the present paper has been very helpful. We thank Pr Thomas Similowski and Dr. Yves Faisandier for fruitful discussions. We also thank Dr. Isabelle Rivals for her helpful comments on the manuscript, Mr. Alexandre Gharbi for its critical readings, and Dr. Tony Maggs for scrutinizing the English language.

References

Bose, A., Lewis, T., Wilson, R., 2005. Two-oscillator model of ventilatory rhythmogenesis in the frog. Neurocomputating 65–66, 751–777.
Brett, S.S., Shelton, G., 1979. Ventilatory mechanisms of the amphibian, *Xenopus laevis*; the role of the buccal force pump. J. Exp. Biol. 80, 269–351.
Broch, L., Morales, R.D., Sandoval, A.V., Hedrick, M.S., 2002. Regulation of the respiratory central pattern generator by chloride-dependent inhibition during development in the bullfrog (*Rana catesbeiana*). J. Exp. Biol. 205, 1161–1169.
Chen, A.K., Hedrick, M.S., 2008. Role of glutamate and substance P in the amphibian respiratory network during development. Respir. Physiol. 162, 24–31.
Gdovin, M.J., Torgerson, C.S., Remmers, J.E., 1998. Neurorespiratory pattern of gill and lung ventilation in the decerebrate spontaneously breathing tadpole. Resp. Physiol. 113, 135–146.
Gustafsson, F., 1996. Determining the initial states in forward–backward filtering. IEEE Trans. Signal Process. 44, 988–992.
Hartelt, N., Skorova, E., Manzke, T., Suhr, M., Mironova, L., Kügler, S., Mironov, S.L., 2008. Imaging of respiratory network topology in living brainstem slices. Mol Cell Neurosci. 37, 425–431.
Horcholle-Bossavit, G., Quenet, B., Foucart, O., 2007. Oscillation and coding in a formal neural network considered as a guide for plausible simulations of the insect olfactory system. Biosystems 89, 244–256.
Izhikevich, E.M., 2003. Simple model of spiking neurons. IEEE Trans. Neural Netw. 14, 1569–1572.
Izhikevich, E.M., 2004. Which model to use for cortical spiking neurons? IEEE Trans. Neural Netw. 15, 1063–1070.
Kogo, N., Perry, S.F., Remmers, J.E., 1994. Neural organisation of the ventilatory active in the frog *Rana castebeiana* I. J. Neurobiol. 25, 1067–1079.
McCulloch, W., Pitts, W., 1943. A logical calculus of the ideas immanent in nervous activity. Bull. Math. Biophys. 7, 115–133.
McLean, H.A., Kimura, N., Kogo, N., Perry, S.F., Remmers, J.E., 1995. Fictive respiratory rhythm in the isolated brainstem of frogs. J. Comp. Physiol. A 176, 703–713.

Oku, Y., Kimura, N., Masumiyaa, H., Okada, Y., 2008. Spatiotemporal organization of frog respiratory neurons visualized on the ventral medullary surface. Respir. Physiol. Neurobiol. 161, 281–290.

Purvis, L.K., Smith, J.C., Koizumi, H., Butera, R.J., 2007. Intrinsic bursters increase the robustness of rhythm generation in an excitatory network. J. Neurophysiol. 7, 1515–1526.

Reid, S.G., Milsom, W.K., 1998. Respiratory pattern formation in the isolated bullfrog (*Rana catesbeiana*) brainstem–spinal cord. Respir. Physiol. 114, 239–255.

Rybak, I.A., Stecina, K., Shevtsova, N.A., McCrea, D.A., 2006. Modelling spinal circuitry involved in locomotor pattern generation: insights from the effects of afferent stimulation. J. Physiol. 577, 641–658.

Sakakibara, Y., 1984. The pattern of respiratory nerve activity in the bullfrog. Jpn. J. Physiol. 34, 269–282.

Taylor, B.E., Harris, M.B., Leiter, J.C., Gdovin, M.J., 2003. Ontogeny of central CO_2 chemoreception: chemosensitivity in the ventral medulla of developing bullfrogs. Am. J. Physiol. Regul. Integr. Comp. Physiol. 285, 1461–1472.

Torgerson, C.S., Gdovin, M.J., Remmers, J.E., 2001a. Sites of respiratory rhythmogenesis during development in the tadpole. Am. J. Physiol. Regul. Integr. Comp. Physiol. 280, 913–920.

Torgerson, C.S., Gdovin, M.J., Brandt, R., Remmers, J.E., 2001b. Location of central respiratory chemoreceptors in the developing tadpole. Am. J. Physiol. Regul. Integr. Comp. Physiol. 280, 921–928.

Vasilakos, K., Kimura, N., Wilson, R.J., Remmers, J.E., 2006. Lung and buccal ventilation in the frog: uncoupling coupled oscillators. Physiol. Biochem. Zool. 79, 1010–1018.

Vasilakos, K., Kimura, N., Wilson, R.J., Remmers, J.E., 2005. Ancient gill and lung oscillators may generate the respiratory rhythm of frogs and rats. J. Neurobiol. 62, 369–385.

Vitalis, T.Z., Shelton, G., 1990. Breathing in *Rana pipiens*: the mechanism of ventilation. J. Exp. Biol. 154, 537–556.

Wang, W., Slotine, J.J.E., 2006. A theoretical study of different leader roles in networks. IEEE Trans. Autom. Contr. 51, 1156–1161.

Wilson, R.J., Vasilakos, K., Harris, M.B., Straus, C., Remmers, J.E., 2002. Evidence that ventilatory rhythmogenesis in the frog involves two distinct neuronal oscillators. J. Physiol. 540, 557–570.

Wilson, R.J., Vasilakos, K., Remmers, J.E., 2006. Phylogeny of vertebrate respiratory rhythm generators: the Oscillator Homology Hypothesis. Respir. Physiol. Neurobiol. 154, 47–60.